Supplementary Information
Universal control of symmetric states using spin squeezing

Nir Gutman[1†], Alexey Gorlach[1†], Offek Tziperman[1], Ron Ruimy[1] and Ido Kaminer[1*]

[1]Technion – Israel Institute of Technology, Haifa 32000, Israel

[†]equal contributors, [*]kaminer@technion.ac.il,

Table of content

The supplementary information derives and supports the claims in the main text. We start by introducing the symmetric states of emitters and the operators that act on them. We continue by introducing the requirements for universal control and prove that a limited set of coherent rotations and squeezing operators is enough for universal control. We then show a bound on the number of steps needed to approximate any operation on symmetric states. Next, we present our optimization algorithm with which we found the exact rotations and squeezing that produce GKP and Schrödinger's cat states. We also summarize the parameters used for the results presented in the figures of the main text. Finally, we discuss the effects of the size of the system on the sequences.

Symmetric operators and their properties

As was done in [1,2], we start by presenting an ensemble of N two-level identical emitters, each existing in the ground state $|\mathrm{g}\rangle$, the exited state $|\mathrm{e}\rangle$, or a superposition thereof. The lowering and raising Pauli operators of the specific system with index i are $\sigma_i^- = |\mathrm{g}\rangle\langle\mathrm{e}|$ and $\sigma_i^+ = |\mathrm{e}\rangle\langle\mathrm{g}|$ accordingly that act on the system with the following relations $\sigma_i^+|\mathrm{g}\rangle = |\mathrm{e}\rangle$, $\sigma_i^-|\mathrm{e}\rangle = |\mathrm{g}\rangle$ and $\sigma_i^-|\mathrm{g}\rangle = \sigma_i^+|\mathrm{e}\rangle = 0$. Another important operator is the diagonal operator $\sigma_i^z = \frac{1}{2}(|\mathrm{g}\rangle\langle\mathrm{g}| - |\mathrm{e}\rangle\langle\mathrm{e}|)$. Each one of these operators acts exclusively on the i^{th} site, with the commutation relations being:

$$\left[\sigma_i^z, \sigma_j^\pm\right] = \mp\delta_{ij}\sigma_i^\pm; \quad \left[\sigma_i^+, \sigma_j^-\right] = -2\delta_{ij}\sigma_i^z. \tag{S1}$$

If we have an ensemble of indistinguishable two-level emitters and we want to remain indistinguishable after an operation, this operation should be applied to the entire system in the same way on all two-level emitters. Only symmetric operations satisfy these conditions and can be constructed from the following basic operations:

$$S_{\pm} = \sum_{i=1}^{N} \sigma_i^{\pm}; \quad S_z = \sum_{i=1}^{N} \sigma_i^{z}. \tag{S2}$$

Since S_+ acting on the ground state $|\mathrm{gg}\ldots\mathrm{g}\rangle$ gives us $\sum_{i=1}^{N} \sigma_i^{\pm} |\mathrm{gg}\ldots\mathrm{g}\rangle = |\mathrm{eg}\ldots\mathrm{g}\rangle + |\mathrm{ge}\ldots\mathrm{g}\rangle + \cdots |\mathrm{gg}\ldots\mathrm{e}\rangle$, it is much more convenient to use the symmetric states:

$$\begin{cases} |N\rangle = |\mathrm{ee}\ldots\mathrm{e}\rangle \\ |N-1\rangle = 1/\sqrt{N}(|\mathrm{ge}\ldots\mathrm{e}\rangle + |\mathrm{eg}\ldots\mathrm{e}\rangle + \cdots |\mathrm{ee}\ldots\mathrm{g}\rangle) \\ \ldots \\ |1\rangle = 1/\sqrt{N}(|\mathrm{eg}\ldots\mathrm{g}\rangle + |\mathrm{ge}\ldots\mathrm{g}\rangle + \cdots |\mathrm{gg}\ldots\mathrm{e}\rangle) \\ |0\rangle = |\mathrm{gg}\ldots\mathrm{g}\rangle \end{cases}.$$

Then, for example, $S_+|0\rangle = \sqrt{N}|1\rangle$. Generally, the lowering or raising operators acting on symmetric state $|m\rangle$ follow the relations:

$$S_+|m\rangle = \sqrt{(m+1)(N-m)}\,|m+1\rangle \triangleq d_+^m|m+1\rangle, \tag{S3a}$$

$$S_-|m\rangle = \sqrt{m(N-m+1)}\,|m-1\rangle \triangleq d_-^m|m+1\rangle, \tag{S3b}$$

$$S_z|m\rangle = (m - N/2)|m\rangle. \tag{S3c}$$

We also note that the commutation relations for the symmetric operators are the same as for Pauli matrices:

$$[S_z, S_{\pm}] = \mp S_{\pm}; \quad [S_+, S_-] = -2S_z. \tag{S4}$$

It is also common to define the operators $S_x = S_+ + S_-$ and $S_y = i(S_- - S_+)$ with commutation relation $[S_x, S_y] = iS_z$.

Conditions for universality

As was shown in [3], to prove that a set of Hamiltonians $\{H_i\}$ promises universal control over the Hilbert space, it is enough to show that the algebra derived from the set spans the entire Hilbert space, i.e., that we can get any operator in the Hilbert space by using linear combinations and commutators of $\{H_i\}$.

First, we prove that the entire Hilbert space of symmetric states of N particles (i.e., the states $|0\rangle, |1\rangle, \ldots |N\rangle$) can be spanned by operating on the ground state $|0\rangle$ with unitary operations corresponding to the Hamiltonians that are the polynomials of S_x and S_y up to order N. A general symmetric state can be written in the symmetric basis $|\psi\rangle = \sum_{n=0}^{N} a_n|n\rangle$. Each term $a_n|n\rangle$ in the sum can be created from the ground state $|0\rangle$ by the operator $a_n/c_n S_+^n$, since $S_+^n|0\rangle = c_n|n\rangle$, where $c_n = \sqrt{n!\,N!/(N-n)!}$. Then $|\psi\rangle = \sum_{n=0}^{N} a_n|n\rangle = \sum_{n=0}^{N} \frac{a_n}{c_n} S_+^n|0\rangle$.

Now we notice that we can build the state $|\psi\rangle = \sum_{n=0}^{N} \frac{a_n}{c_n} S_+^n |0\rangle$ by applying infinitesimal unitary operations $e^{\alpha_1 S_+ - \alpha_1^* S_-}$ on $|0\rangle$, where α_1 is a complex number such that $|\alpha_1| \ll 1$. Applying this unitary operation, we get:

$$e^{\alpha_1 S_+ - \alpha_1^* S_-}|0\rangle \approx |0\rangle + \alpha_1 S_+|0\rangle = |0\rangle + \alpha_1 c_1|1\rangle.$$

Then applying the same operator M_1 times yields:

$$\left(e^{\alpha_1 S_+ - \alpha_1^* S_-}\right)^{M_1}|0\rangle \approx |0\rangle + \alpha_1 M_1 c_1|1\rangle.$$

We can choose $\alpha_1 M_1 = a_1/(a_0 c_1)$ and get $\left(e^{\alpha_1 S_+ - \alpha_1^* S_-}\right)^{M_1}|0\rangle \approx |0\rangle + \frac{a_1}{a_0}|1\rangle$. In this way, we were able to construct the coefficient of $|1\rangle$ in the wavefunction $|\psi\rangle$. To construct the coefficient of $|n\rangle$, we apply M_n times the following unitary operator:

$$\left(e^{\alpha_n S_+^n - \alpha_n^* S_-^n}\right)^{M_n}|0\rangle \approx |0\rangle + \alpha_n M_n c_n|n\rangle.$$

Then we can choose $\alpha_n M_n = a_n/(a_0 c_n)$. Thus, by following this construction, we can build an arbitrary symmetric state $|\psi\rangle$:

$$\left(e^{\alpha_N S_+^N - \alpha_N^* S_-^N}\right)^{M_N} \ldots \left(e^{\alpha_2 S_+^2 - \alpha_2^* S_-^2}\right)^{M_2} \left(e^{\alpha_1 S_+ - \alpha_1^* S_-}\right)^{M_1}|0\rangle \xrightarrow[\{a_i\}_{i=1}^N \to 0]{} |0\rangle + \frac{a_1}{a_0}|1\rangle + \cdots \frac{a_n}{a_0}|N\rangle \propto |\psi\rangle.$$

This set of unitary operators corresponds to the Hamiltonians that are polynomials in $S_\pm = \frac{S_x \pm i S_y}{2}$ up to the N^{th} order. Consequently, if we can construct any Hamiltonian that is an arbitrary polynomial in S_x and S_y, then we can generate any pure symmetric state.

Proof of universality

Let us now discuss harmonic oscillators and the symmetric states of emitters. Both models contain coherent rotations and squeezing operations. However, as we will show below, only in two-level identical emitters squeezing and coherent rotations are enough for the universality, while for the harmonic oscillator, these operations can only create Gaussian states.

Coherent rotations and squeezing do not constitute universal control over the states of the harmonic oscillator: Coherent rotations are the operators x and p and any linear combination thereof in a quadrature. Together with the 2nd "squeezing" operators x^2, p^2 and $s = (xp + px)/2$, we get the set $\{x, p, x^2, p^2, s\}$. As was shown in [4], we start by writing some commutation relations. Two 1st order operators give a 2nd order commutation relation $[x, p] = i\hbar$ that yields a 0th order scalar. The 2nd order operator s with both 1st order operators x and p yields the 3rd order commutation relations $[s, p] = -p$ and $[s, x] = -ix$, both yielding 1st order operators. Thus, we conclude that we can construct Hamiltonians that are quadratic in x and p and not higher. We do not span the entire Hilbert space and thus cannot achieve universal control.

Coherent rotations and squeezing constitute universal control over the symmetric states of emitters: In contrast to the previous system, here the coherent rotations are operators $S_x = S_+ + S_-$ and $S_y = i(S_- - S_+)$ with commutation relation $[S_x, S_y] = iS_z$. Already we see a stark contrast from the previous case. The commutation relation of two 1st-order operators yields a 1st-order operator. Introducing squeezing S_x^2 and S_y^2 allows us to reach the commutation relations $[S_x, S_y^2] = i(S_z S_y + S_y S_z) = S_x + iS_y S_z$. So, by subtracting S_x we can get the operator $S_y S_z$. The same can be done with $[S_z, S_y^2]$ and $[S_y, S_x^2]$ to get $S_x S_y$ and $S_x S_z$. Now, since we already possess $S_y S_z$ and can incorporate it into the commutation relation, we get $[S_x, S_y S_z] = i(S_z^2 - S_y^2)$. Combining the other operators achieved so far, we see that the algebra contains all polynomials of S_x, S_y and S_z of the 2nd power.

With all the 2nd power operators in hand, we can also construct any 3rd power operator, and with them all 4th power operators and so on using the following inductive proof:
Assume that we can already reach S_x, S_y and S_z to some powers n, m and k respectively, we can then use commutation relations to get:

$$[S_x, S_y^m] = i\sum_{i=1}^{m} S_y^{i-1} S_z S_y^{m-i} = iS_y^{m-1} S_z + \text{lower orders}$$

$$[S_x^2, S_y^m] = S_x[S_x, S_y^m] + [S_x, S_y^m]S_x = i\sum_{i=1}^{m} S_x S_y^{i-1} S_z S_y^{m-i} + i\sum_{i=1}^{m} S_y^{i-1} S_z S_y^{m-i} S_x$$
$$= iS_x S_y^{m-1} S_z + \text{lower orders}$$

Thus:

$$[S_x^2, S_x^n S_y^m S_z^k] = S_x^n [S_x^2, S_y^m] S_z^k + S_x^n S_y^m [S_x^2, S_z^k]$$
$$= iS_x^{n+1} S_y^{m-1} S_z^{k+1} + iS_x^{n+1} S_y^{m+1} S_z^{k-1} + \text{lower orders} \quad \text{(S5a)}$$

$$[S_y^2, S_x^n S_y^m S_z^k] = iS_x^{n-1} S_y^{m+1} S_z^{k+1} + iS_x^{n+1} S_y^{m+1} S_z^{k-1} + \text{lower orders} \quad \text{(S5b)}$$

$$[S_z^2, S_x^n S_y^m S_z^k] = iS_x^{n-1} S_y^{m+1} S_z^{k+1} + iS_x^{n+1} S_y^{m-1} S_z^{k+1} + \text{lower orders} \quad \text{(S5c)}$$

Combining the formulas yields $[S_x^2, S_x^n S_y^m S_z^k] + [S_y^2, S_x^n S_y^m S_z^k] - [S_z^2, S_x^n S_y^m S_z^k] = 2iS_x^{n+1} S_y^{m+1} S_z^{k-1} + \text{lower orders}$, effectively raising the power of S_x and S_y by 1 while only lowering the power of S_z by 1, thus achieving a set of operators higher in overall polynomial order than what we have started with. With different linear combinations, we can also get:

$$S_x^{n+1} S_y^{m+1} S_z^{k-1}, \qquad S_x^{n+1} S_y^{m-1} S_z^{k+1}, \qquad S_x^{n-1} S_y^{m+1} S_z^{k+1},$$

because any polynomial of S_x, S_y and S_z is reachable with enough mixing of the commutation relations and linear combination of them. The power to reach any polynomial promises universal control.

Complexity

With the proof that any unitary acting on symmetric states can be created using the simple set of coherent rotations and squeezings $\{S_x, S_y, S_z, S_x^2, S_y^2\}$, a sensible question would be to ask how many such operations are needed to construct an arbitrary unitary operator. This, of course, will vary depending on the desired operator, so a better query will be to find a cap on the number of operations needed. In this section, we prove the needed number of operations to be polynomial in the number of emitters N, and in fact, show it to be $O(N^4)$.

Given a set of Hamiltonians $\{S_x, S_y, S_z, S_x^2, S_y^2\}$, we can construct an arbitrary product of the following operators $e^{-i\alpha S_{x,y,z}}, e^{-i\beta S_{x,y}^2}$ for arbitrary α and β. To effectively construct the unitary operator that is generated from the addition of Hamiltonians A and B, we need $2k$ such operators, where k is an integer with which greater accuracies can be achieved:

$$e^{-i(A+B)t} = \left(e^{-\frac{iAt}{k}} e^{-\frac{iBt}{k}}\right)^k + O\left(\frac{1}{k}\right).$$

To build the unitary generated from the commutation of A and B, we need $4k$ operators:

$$e^{-i[B,A]t} = \left(e^{-iA\sqrt{\frac{t}{k}}} e^{-iB\sqrt{\frac{t}{k}}} e^{iA\sqrt{\frac{t}{k}}} e^{iB\sqrt{\frac{t}{k}}}\right)^k + O\left(\frac{1}{k}\right).$$

Now let us calculate how many operations we need to construct a desired unitary operator $U_i = e^{-iH_i t}$. We can examine what happens when this unitary acts on the ground state and notice that we will get some symmetric state $|\psi_i\rangle = e^{-iH_i t}|0\rangle \approx (1 - iH_i t)|0\rangle$. Since $|\psi_i\rangle$ can be decomposed into the symmetric basis as $|\psi_i\rangle = \sum_{n=0}^{N} a_n |n\rangle = \sum_{n=0}^{N} a_n S_+^n |0\rangle$, we find that H_i can be decomposed into powers of S_+ operator up to S_+^N (the higher powers of S_+ all give zero). This puts a cap of N on the degree of the polynomial of S_x, S_y, S_z in each Hamiltonian H_i, i.e.:

$$H_i = \sum_{n=0}^{N} \sum_{k=0}^{n} \sum_{m=0}^{n-k} c_{nmk}\, S_x^{n-k-m} S_y^k S_z^m. \tag{S6}$$

For each degree n from 0 to N in (S6), the number of operators with this degree is $\sum_{k=0}^{n} \sum_{m=0}^{n-k} 1 = \frac{1}{2}(n+1)(n+2) \in O(n^2)$.

We showed universality using a proof by induction, where a polynomial of S_x, S_y, S_z with degree n can be constructed by using $O(n)$ commutation relations, i.e., with $O(n \cdot k)$ unitary operations, using polynomials of lower degrees $(n-1, n-2, \ldots, 2, 1)$.

To get all polynomials of degree n, we need only $O(n^3 \cdot k^3)$ operators of lower degrees, and thus $O(N^4 \cdot k^3)$ operators to get all polynomials up to degree N. Hence, the overall number of operators from the set $\{S_x, S_y, S_z, S_x^2, S_y^2\}$ needed to construct any unitary in the Hilbert space of symmetric states of N emitters is $O(N^4 \cdot k^3)$. Thus, we proved that any unitary acting in the basis of symmetric states can be achieved by applying $O(N^4 \cdot k^3)$ operations from the set of symmetric

operators $\{S_x, S_y, S_z, S_x^2, S_y^2\}$. To get good precision one needs a large enough k, however, the number of operations even for large k still scales as N^4. In practice, many interesting states can be achieved with even fewer operations, as we have shown in the main text.

Optimization protocol

The optimization algorithm's purpose is to find the optimal parameters for the sequence that results in a state with maximal fidelity with respect to the target state: $\text{fidelity}\left(\rho_{\text{target}}, \rho(\vec{\theta})\right)$, where the set of parameters $\vec{\theta}$ control the different unitary operations at each time step towards the final state. The parameter space is filled with local minima, which greatly hinders most gradient-descent-based optimization methods.

To overcome this difficulty, we introduce two random processes into our method. Firstly, the process of optimization begins with the generation of many independent random guesses as the initial starting parameters. Secondly, for each such set of initial parameters, we repetitively start an optimization instance of the Nelder-Mead method [5], where some of the parameters are locked and do not participate in the optimization method. This allows us to sometimes skip over some local minima, hoping eventually to converge into the global minimum.

The Nelder-Mead method was chosen because it was the only readily available method that proved to find local minima in our system while incorporating the constraints that we deemed necessary (e.g., limiting the angles of rotations to the range $[-\pi, \pi]$) and does not require knowledge of the exact derivatives. We believe that if an exact derivative can be computed for any parameter in the sequence of pulses, a better optimization method could have been chosen.

Each step consists of rotation and squeezing. A rotation pulse is parametrized by three independent parameters $\Omega_{x,y,z}$ of rotations around $\hat{x}, \hat{y}$ and $\hat{z}$ axes: $R_{\hat{n}}(\theta) = \exp\left(i\left(\Omega_x S_x + \Omega_y S_y + \Omega_z S_z\right)\right)$ or equivalently by the unit vector $\hat{n}$ and the rotation angle θ around it:

$$R_{\hat{n}} = \exp\left(i\left(n_x S_x + n_y S_y + n_z S_z\right)\theta\right), \tag{S7}$$

where $n_{x,y,z} = \Omega_{x,y,z}/\sqrt{\Omega_x^2 + \Omega_y^2 + \Omega_z^2}$ and $\theta = \sqrt{\Omega_x^2 + \Omega_y^2 + \Omega_z^2}$. The squeezing is described by the following operation:

$$S(\alpha, \beta) = \exp\left(i\left(\alpha S_x^2 + \beta S_y^2\right)\right). \tag{S8}$$

The number of required steps N is a hyperparameter, unknown before finding the best solution. To find it, we always start with only two pulses, exhaustively try many initial guesses until it seems that a better fidelity cannot be achieved, and only then increase N by 1. When adding another step of rotation and squeezing to the sequence (thus, increasing N), we initialize all its parameters to 0. Which acts the same as adding the identity operator. This allows us to add the

new step in the middle (or even beginning) of the sequence, giving the algorithm a richer parameter space to work with, while not losing any progress gained thus far.

For each rotation, we have three parameters and for each squeezing pulse, we have two parameters – overall five free parameters for each step plus three parameters for a final rotation, giving:

$$\text{Number of Parameters} = 5 \cdot N + 3. \tag{S9}$$

For typical values of N in the main text, this means having above ~30 parameters, and thus most derivative-less methods will struggle to converge on a global minimum in a parameter space filled with local minima. This is the reason why we introduced the second random process of freezing part of the parameters while letting the others take part in the optimization process. We have found that a good number of free parameters is ~20. This is also crucial to allow new pulses to be added in the middle of a sequence: Add a new pulse with all zero initial parameters, freeze most parameters besides the new ones, and start a new optimization instance.

Parameters used in the numerical simulations

Here we write explicitly the parameters that are needed to replicate the results shown in the main paper. The rotation parameters at each step are: $\hat{n}_i$ for the rotation axis and θ_i for the degree of rotation (in radians). The squeezing in directions $\hat{x}$ and $\hat{y}$ are α_i and β_i respectively. In the cat codes, we write $|\gamma\rangle = e^{-\frac{1}{2}|\gamma|^2} \sum_{n=0}^{\infty} \frac{\gamma^n}{\sqrt{n!}} |n\rangle$ for a coherent state written in the symmetric basis, with a complex parameter γ.

2-legged Schrödinger's cat: $|2\text{cat}\rangle = |\gamma\rangle + i|-\gamma\rangle$, where $\gamma = 3$.

Table 1: operators for 2-legged cat creation for $N = 40$

step #	$\hat{n}$			θ	α	β
1	0.44683	0.21351	0.86876	3.73127	1.57143	1.57017
end	0.00000	0.00000	1.00000	2.35948		

4-legged Schrödinger's cat: $|4\text{cat}\rangle = |\gamma\rangle + e^{i\phi}|+i\gamma\rangle + e^{i2\phi}|-\gamma\rangle + e^{i3\phi}|-i\gamma\rangle$, where $\gamma = 3$ and $\phi = \pi/4$.

Table 2: operators for 4-legged cat creation for $N = 40$

step #	$\hat{n}$			θ	α	β
1	0.220058	0.789986	-0.57227	4.061466	0.003675	-0.7836
end	0.614706	0.530748	-0.58347	4.24025		

Hexagonal GKP with 10 dB squeezing.

Table 3: operators for hexagonal GKP creation for $N = 40$

step #	$\hat{n}$			θ	α	β
1	0.58422	-0.70216	0.40701	3.73793	-0.01883	0.10958
2	0.12109	0.76554	0.63189	3.51680	0.56324	0.06183
3	-0.99588	0.03711	0.08277	3.16463	-0.46139	0.24754
4	0.55086	0.73301	-0.39905	0.81578	0.01654	0.05930
5	0.63164	0.09674	0.76920	0.46043	0.00749	0.01291
6	0.17495	0.05641	-0.98296	1.17352	0.01198	0.02608
7	0.69954	-0.23653	-0.67431	3.11339	3.15159	-0.01382
8	0.70298	-0.64758	-0.29404	0.99739	-1.37202	0.03684
9	0.89993	0.00384	0.43603	0.77684	0.52291	0.25252
10	0.89155	0.38970	-0.23081	0.41266	3.07564	0.79775
11	0.05450	0.33542	0.94049	1.54108	0.24451	1.06955
end	0.92003	0.38822	-0.05321	3.42003		

Square GKP with 10 dB squeezing.

Table 4: operators for square GKP creation for $N = 40$

step #	$\hat{n}$			θ	α	β
1	-0.00355	0.307337	-0.95159	0.396325	0.024936	0.227007
2	-0.01773	0.230252	-0.97297	1.090371	0.002457	0.21566
3	0.200697	0.978824	-0.0403	0.159439	-0.00392	-0.06637
4	0.806244	-0.36774	0.463401	3.038831	-0.04836	-0.29011
5	-0.63756	0.630441	-0.44278	3.500829	-1.10497	-0.24593
6	0.020905	-0.92403	-0.38174	2.812456	0.028772	-0.11394
7	-0.76349	-0.62554	0.160584	0.350578	0.40291	0.167819
8	0.96056	-0.14113	-0.2396	1.718151	-0.00775	0.103055
9	0.854513	0.223536	0.46887	0.770651	0.044993	-0.06539
10	0.218843	-0.92957	0.296648	0.256411	-0.08197	0.049369
11	0.321551	-0.6716	-0.6675	0.506597	-0.30929	0.992603
end	-0.00781	-0.66735	0.744704	1.456135		

Some parameters appear in higher precision in the code.

Size and scalability of the system

The generation of different quantum states depends on the number of emitters and on the number of steps used in our algorithm to reach the optimal operation parameters. Each such quantum state can be described by a Wigner function on the Bloch sphere. The Wigner function is limited to a sphere because there are only $N+1$ symmetric states that arise from N indistinguishable emitters, rather than the infinite number of states of the harmonic oscillator. This comparison is linked to the difference between coherent rotations and displacements. Whereas coherent rotations on symmetric states are limited by the size of the Bloch-sphere they reside on, the displacement operators on states of the harmonic oscillator can move coherent states to any position $|\alpha\rangle$, even infinitely far away from $|0\rangle$.

Coherent rotations that rotate states close to the bottom of the sphere are similar to displacements on the infinite plane of a harmonic oscillator. But using the top of the sphere is unique to a system of emitters. Thus, the sequence of unitary transformation leading to the target symmetric state is strongly dependent on the number of emitters in the system (i.e., the size of the sphere) (Tables 5-9).

The target photonic state that we expect being emitted from the target emitters' state can be written in terms of the density matrix:

$$\rho_{\mathrm{ph}} = \sum_{n,m=0}^{+\infty} \rho_{\mathrm{ph}}^{(n,m)} |n\rangle\langle m| , \tag{S7}$$

where $|n\rangle$ is the Fock state with n photons. The corresponding emitters' state on the sphere for N emitters is then described by:

$$\rho_{\mathrm{sym}} = \sum_{n,m=0}^{N} \rho_{\mathrm{sym}}^{(n,m)} |n\rangle\langle m| , \tag{S8}$$

where $|n\rangle$ is the symmetric state with n excitations. The larger the number of emitters N, the closer it is to the target photonic state (except for the states near the top). The density matrices become almost identical when the maximum number of photons in Eq. (S7) is much less than N. Fig. S1 shows the fidelity between a GKP state on the sphere $\rho_{\mathrm{sym}}^{(n,m)}$ and the GKP photonic state with 10 dB squeezing $\rho_{\mathrm{ph}}^{(n,m)}$, depending on the number of emitters N. According to this figure, we need to have approximately 20 emitters for 95% fidelity with the photonic GKP state. Unfortunately, it is easier to operate on a small number of emitters. Thus, one would like to find an optimal number of emitters N, which is large enough to have high fidelity with the photonic state but small enough to require a smaller number of operations.

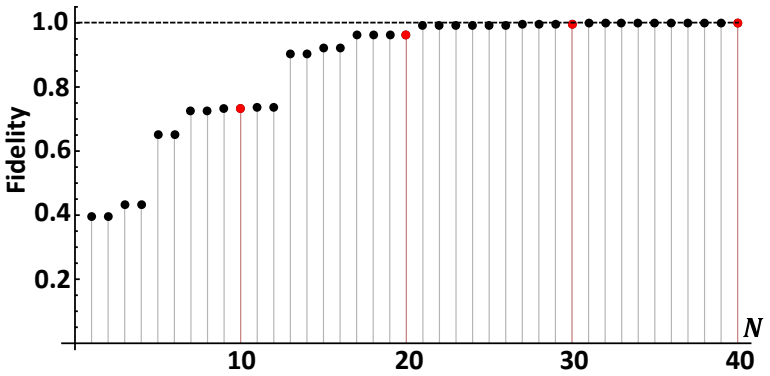

Fig. S1: Dependence of the fidelity on the number of the emitters N. The fidelity between photonic GKP with 10 dB squeezing and the corresponding symmetric state, calculated as a function of N. The red dots show the fidelities for the cases of $N = 10, 20, 30, 40$ that are further analyzed below.

We investigate in detail the creation of the GKP square state for $N = 10, 20, 30, 40$ emitters. The tables below present the operations found by our algorithm to create the GKP square state.

Table 5: operators for square GKP creation for $N = 10$

step #	$\hat{n}$			θ	α	β
1	0.000132	0.42548	-0.90496	1.09692	0.029659	0.66818
2	-0.18694	-0.72809	-0.65949	1.70843	0.11434	0.69204
3	0.16916	0.98295	0.071944	2.51638	-0,14641	-0.35958
end	-0.093022	-0.9912	-0.094139	2.77622		

Table 6: operators for square GKP creation for $N = 20$

step #	$\hat{n}$			θ	α	β
1	0.34882	0.93269	-0.091643	0.37996	0.020952	0.30676
2	-0.00124	0.24714	-0.96897	1.3652	0.039762	0.20592
3	0.11709	-0.016928	-0.99297	0.058132	0.046752	-0.10915
4	0.72803	-0.31639	0.60816	2.9472	-0.035026	-0.27228
5	-0.61714	0.62604	-0.47665	3.6542	-1.1362	-0.26776
6	0.00213	-0.91428	-0.40507	2.6185	0.062408	-0.16803
end	0.029708	-0.6867	0.72625	1.70724		

Table 7: operators for square GKP creation for $N = 30$

step #	$\hat{n}$			θ	α	β
1	0.28652	-0.77133	-0.56827	0.12957	0.021638	0.24041
2	-0.03515	0.2694	-0.96238	1.13090	0.016643	0.22389
3	-0.12158	0.99171	0.041382	0.13527	-0.018776	-0.07851
4	0.82069	-0.32264	0.47154	2.9581	-0.04390	-0.28774
5	-0.60712	0.67159	-0.42469	3.29423	-1.10446	-0.24192
6	0.040669	-0.87993	-0.47335	2.58678	0.09838	-0.14025
7	-0.39717	-0.90114	0.17374	0.22491	0.40805	0.16609
8	0.96508	-0.10164	-0.24139	1.72135	0.00371	0.14857
9	0.83186	0.34694	0.43316	0.90499	0.07968	-0.07040
10	0.09887	-0.98716	-0.12542	0.24233	-0.09011	0.05597
11	0.26079	-0.66078	-0.70381	0.55102	-0.33873	0.99373
end	-0.00959	-0.77069	0.63713	1.68454		

Table 8: operators for square GKP creation for $N = 40$

step #	$\hat{n}$	θ	α	β

1	-0.00355	0.307337	-0.95159	0.396325	0.024936	0.227007
2	-0.01773	0.230252	-0.97297	1.090371	0.002457	0.21566
3	0.200697	0.978824	-0.0403	0.159439	-0.00392	-0.06637
4	0.806244	-0.36774	0.463401	3.038831	-0.04836	-0.29011
5	-0.63756	0.630441	-0.44278	3.500829	-1.10497	-0.24593
6	0.020905	-0.92403	-0.38174	2.812456	0.028772	-0.11394
7	-0.76349	-0.62554	0.160584	0.350578	0.40291	0.167819
8	0.96056	-0.14113	-0.2396	1.718151	-0.00775	0.103055
9	0.854513	0.223536	0.46887	0.770651	0.044993	-0.06539
10	0.218843	-0.92957	0.296648	0.256411	-0.08197	0.049369
11	0.321551	-0.6716	-0.6675	0.506597	-0.30929	0.992603
end	-0.00781	-0.66735	0.744704	1.456135		

Indeed, we can see that for different numbers of emitters, we should perform different sets of operations to get the GKP state. It is likely that these differences are because our algorithm converges to a set of parameters that are very sensitive to the number of emitters N, and thus different parameters are found for each N. Furthermore, the number of required steps increases for larger N: while to create GKP with $N = 40$ or $N = 30$ we need to have 11 steps, GKP with $N = 20$ can be created in just 6 steps, and GKP with $N = 10$ can be created in just 3 steps. This result highlights the effectiveness of our method compared to other methods for both small and large numbers of emitters. For a small number of emitters, e.g., $N = 10$, we just need 3 steps to create the best approximation of a GKP state that can be created with just 10 emitters (whose fidelity to the true GKP state is 75%). In comparison, with ordinary single qubit and CNOT gates, at least N(=10) gates are needed to create the same state, since it requires all to all entanglement (often the number of gates is even larger, scaling as 2^N). For a larger number of emitters, e.g., $N = 40$, we get close to the perfect GKP state in the emission. However, a large number of emitters are more prone to decohere (more details in the next section). Nevertheless, our method even for larger N should be more efficient than conventional single-qubit and two-qubit gates. The optimized GKP states for $N = 10,20,30,40$ emitters are presented in Fig. S2.

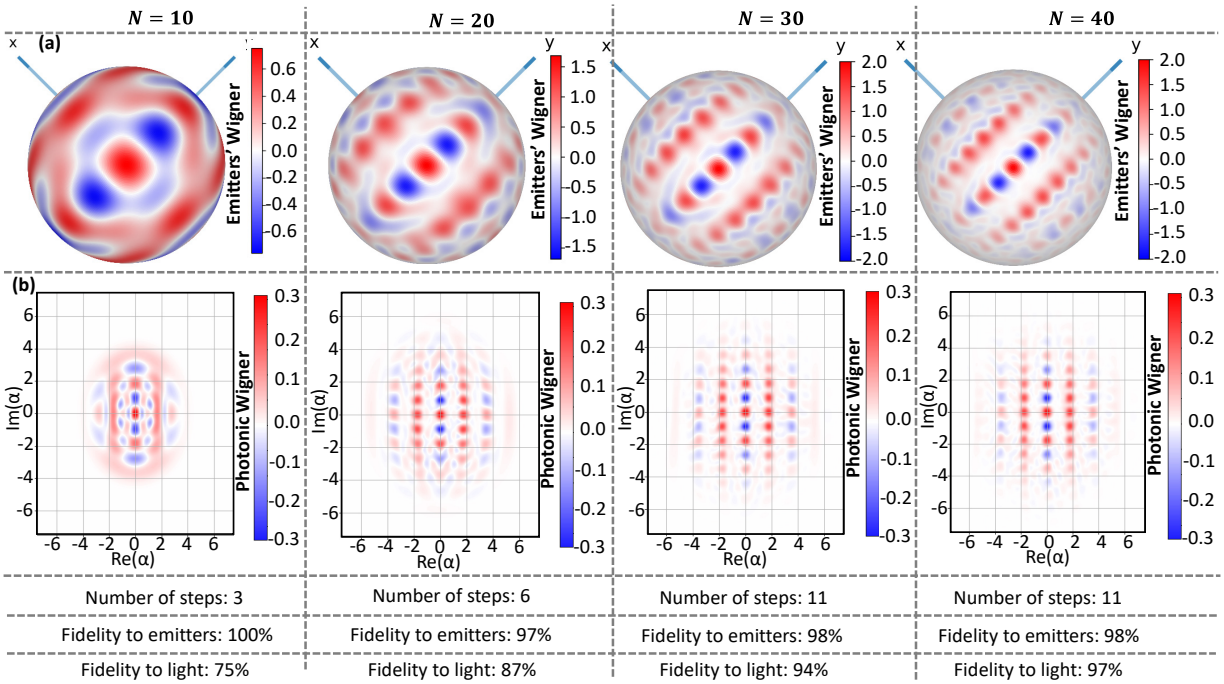

Fig. S2: GKP state creation for different numbers of emitters: $N = 10, 20, 30, 40$. (a) The created GKP states on the sphere according to the operations described in Tables 5-8 above. The optimal operations are found using the optimization algorithm described in the previous section. **(b)** The corresponding emitted photonic state from the created symmetric state on the sphere. Under the panels, we summarize the number of steps needed to achieve the corresponding state, the corresponding fidelity to the target symmetric state of the emitters described by Eq. (S7), and the fidelity of the resulting emission compared and the target photonic GKP state. The fidelity grows for a larger number of emitters, while requiring a larger number of steps to reach the optimal operation parameters.

We can deduct two key statements from the results: First, the limited number of symmetric states plays a key role in our ability to achieve universal control using such a small set of operators. Similarly, the smaller the system, the fewer operations we need to get an arbitrary symmetric state. Second, we get entirely different results for different system sizes. Fig. S3 shows how the same sequence can result in entirely different final states when the size of the system varies.

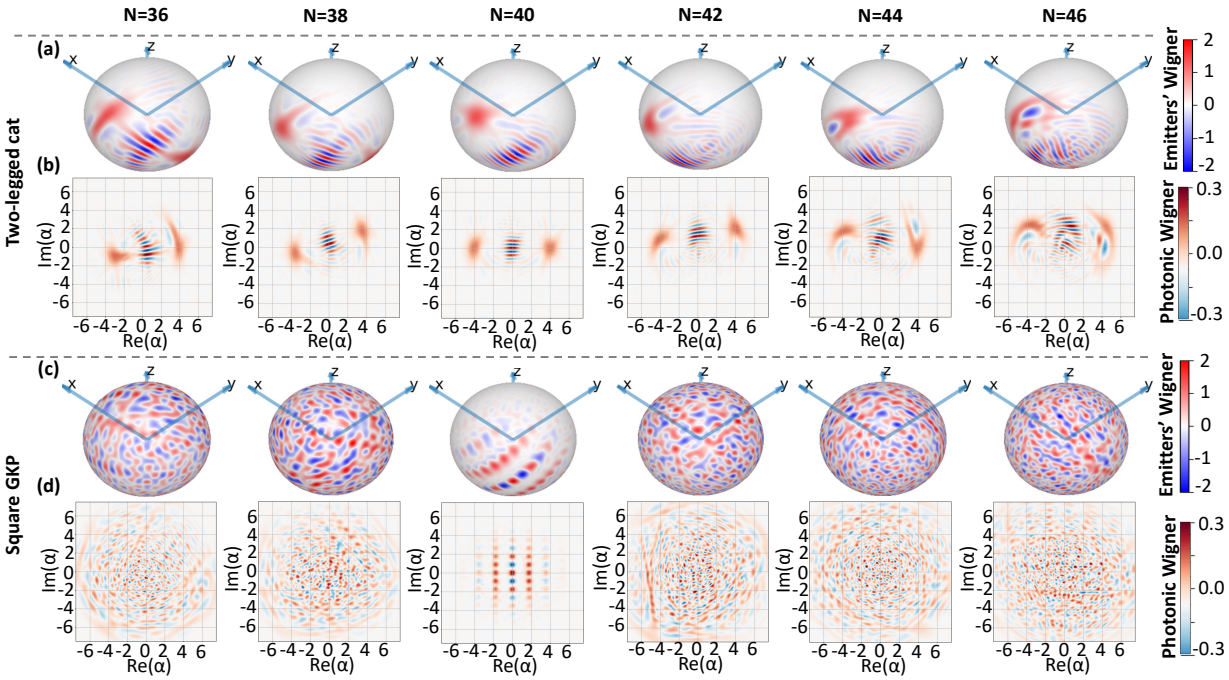

Fig. S3: The dependence of the sequence on the number of emitters: Final states created for different numbers of emitters N, using the fixed parameters learned for a system with $N = 40$ emitters. **(a-b)** The resulting emitters' Wigner states on the Bloch-sphere and the corresponding Wigner functions of the emitted photonic states, for a sequence optimized to create a 40-emitters two-legged cat. The resulting states strongly vary when changing the number of emitters, but still resemble to desired two-legged cat. **(c-d)** The same results but optimized to create a square-GKP state. Unlike with the case of the cat state, here the resulting states no longer resemble the target square-GKP state, showing a greater sensitivity to the number of emitters. The reason for the relative robustness of the scheme in the case of the cat state is that the Wigner function of the emitters remains close to the bottom of the sphere during the sequence of operations. Thus, the size of the system does not affect the result as much as for the sequence optimized for a square-GKP, which involves states on the spheres much farther from the bottom.

Decoherence in the quantum state transfer

This section considers decoherence during the quantum state transfer from emitters to photonic state. We consider the decays that occur to unwanted modes. These manifest in different platforms, such as emitters (e.g., superconducting qubits) coupled to the waveguide (e.g., transmission line) that not only emit superradiance into the waveguide but also emit into other individual decay channels. Another example platform is neutral atoms trapped in a cavity, which due to the microscopic distances between them, can emit to the side of the cavity, which result in their individual decay channels. We consider the action of the decay channels only during the emission, because during the excitation, this type of decay is negligible (see the next section).

The dynamics of the emitters' system during the emission is described by the Lindblad equation:

$$\frac{d\rho}{dt} = \Gamma_{\text{emission}}\left(S_-\rho S_+ - \frac{1}{2}\{S_+S_-,\rho\}\right) + \Gamma'\sum_n\left(\sigma_-^n\rho\sigma_+^n - \frac{1}{2}\{\sigma_+^n\sigma_-^n,\rho\}\right), \tag{S10}$$

where Γ_{emission} is the superradiant emission to the correct channel, and Γ' is the sum of all individual unwanted decays. The solution for the resulting emitted photonic state is described in detail in [6,7]. Fig. S3 presents the results of the simulation with $N = 6$ emitters initially prepared in cat states, showing the fidelity between the emitted photonic state with unwanted decay channels and the ideal cat state. The simulations are numerically demanding, thus done for a small number of emitters ($N = 6$) and only for cat states. Nevertheless, the results show that the fidelity to the ideal state is high if the sum of decay rates to unwanted channels is smaller than the rate of emission into the wanted mode Γ_{emission} (which can be enhanced by superradiance).

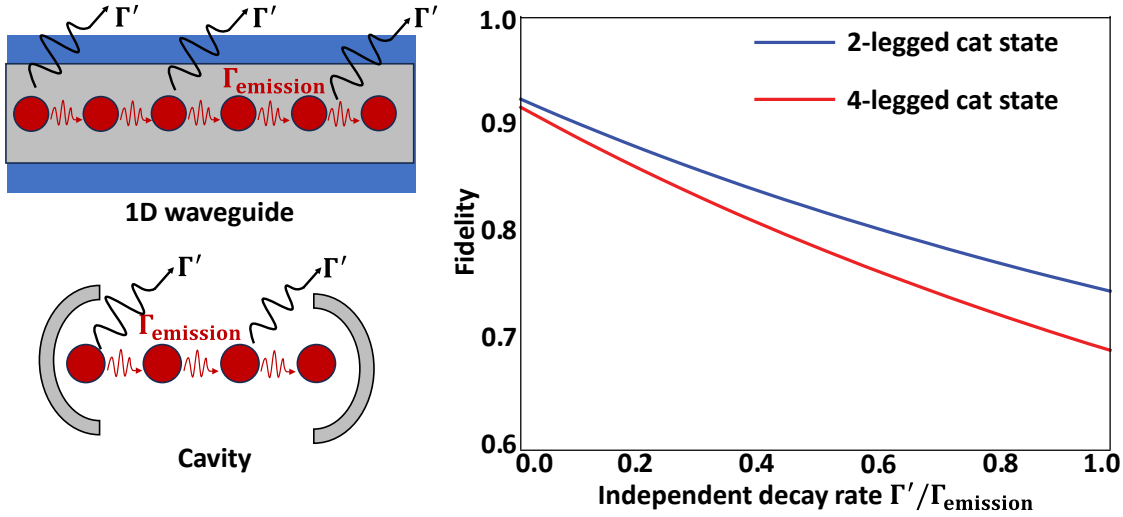

Fig. S3: Influence of unwanted decay channels on the emitted photonic state. The fidelity between the emitted photonic state with unwanted decay channels and an ideal cat state, as the function of Γ'. For this plot, the initial states are chosen as 2-legged and 4-legged cat states with the number of emitters being $N = 6$.

Decoherence in the preparation stage

In any physical implementation of our protocol, some form of decoherence is inevitable. In the previous section, we considered the emitters' individual decay due to their coupling to modes other than the superradiant mode. This effect is crucial during the emission process. Here, we consider the effect of the dephasing, which will hurt the emitter state fidelities during the preparation stage. To model the effects of dephasing, we use a modified master equation, adding independent dephasing channels:

$$\frac{\partial \rho}{dt} = -i[H, \rho] + \Gamma_{\text{D}} \sum_{n} (\sigma_z^n \rho \sigma_z^n - \rho)\,, \tag{S10}$$

where Γ_{D} is the rate of the dephasing, $H = \omega_0 S_z + H_{\text{op}}$, where H_{op} includes all the operations, considering combinations of linear S_x, S_y, S_z and quadratic S_x^2, S_y^2 terms. The strength of these Hamiltonians is taken from real experimental capabilities for superconducting qubits, trapped ions and Rydberg atoms. For superconducting qubits, the strength of squeezing is around 60 MHz; the time of the dephasing for superconducting qubits is around 2 μs [8]. In the case of trapped ions,

the squeezing strength is around 1 kHz, and the dephasing time is around 15 ms [9]. For Rudberg atoms, the dephasing time is 1 μs, and the strength of spin-squeezing operations is around 1 MHz, respectively [10]. The dephasing times of trapped ions, superconducting and Rudberg atom qubits are shown in Fig. S5 with dashed lines. Fig. S5 shows the fidelity between the state without and with dephasing for the creation of the two-legged cat state and the square GKP state for $N = 40$.

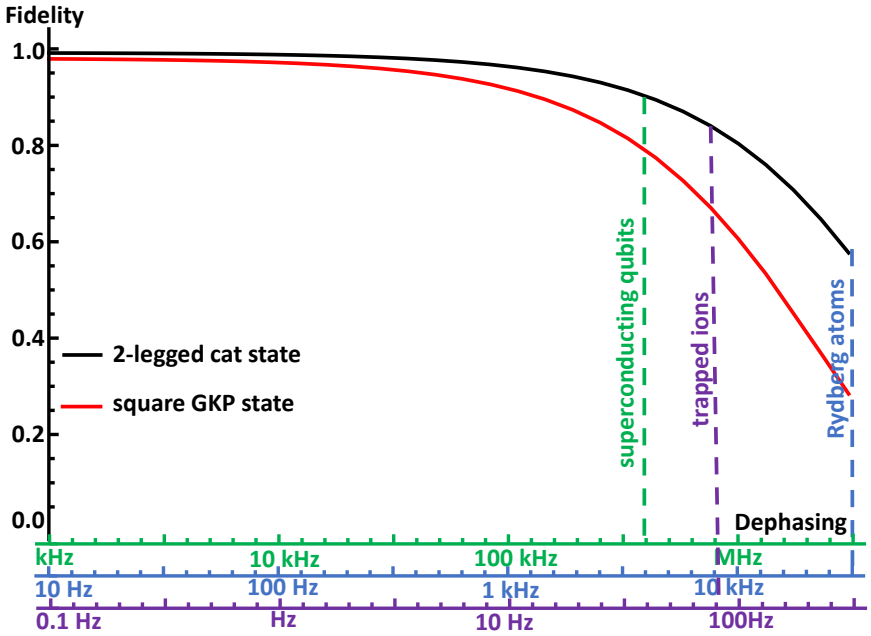

Fig. S5: The effect of dephasing on the creation of an arbitrary symmetric state. We simulate Eq. (S10) and find the fidelity between the state generated without and with dephasing. We take the parameters from [8] for superconducting qubits, from [10] for Rydberg atoms, and from [9] for trapped ions. Three x-axes are marked for the three platforms, each with a dashed vertical line marking an example working point based on the corresponding paper. We present two curves: for a short preparation, based on creating a 2-legged cat state (just 1 step), and for a long preparation, based on creating a square GKP state (11 steps). For all the cases, we assumed the same ratio in strength of coherent rotations and squeezing to be 30 (the number is taken from [8]). The number of emitters in the simulation is taken to be $N = 40$.

These numerical simulations show that our proposed protocol is feasible on existing platforms. For superconducting qubits, we find a fidelity of 90% for cat and 80% for GKP. The fidelities are lower for trapped ions and Rydberg atoms due to shorter decoherence time. However, slight improvements in these platforms should pave the way for creating GKP and cat states in the optical regime. Still, we find fidelities of 60% and 30% for cat and GKP states respectively in Rydberg atoms and 85%, 65% for trapped ions.

References:

[1] M. Gross and S. Haroche, *Superradiance: An Essay on the Theory of Collective Spontaneous Emission*, Phys Rep **93**, 301 (1982).

[2] R. Bonifacio, P. Schwendimann, and F. Haake, *Quantum Statistical Theory of Superradiance. I*, Phys Rev A **4**, 302 (1971).

[3] S. Lloyd, *Almost Any Quantum Logic Gate Is Universal*, Phys Rev Lett **75**, 346 (1995).

[4] S. Lloyd and S. L. Braunstein, *Quantum Computation over Continuous Variables*, Phys Rev Lett **82**, 1784 (1999).
[5] J. A. Nelder and R. Mead, *A Simplex Method for Function Minimization*, Comput J **7**, 308 (1965).
[6] A. H. Kiilerich and K. Mølmer, *Input-Output Theory with Quantum Pulses*, Phys Rev Lett **123**, (2019).
[7] O. Tziperman, G. Baranes, A. Gorlach, R. Ruimy, M. Faran, N. Gutman, A. Pizzi, and I. Kaminer, *Spontaneous Emission from Correlated Emitters*, in *ArXiv:2306.11348* (2023).
[8] C. Song et al., *Generation of Multicomponent Atomic Schrödinger Cat States of up to 20 Qubits*, Science **365**, 574 (2019).
[9] J. G. Bohnet, B. C. Sawyer, J. W. Britton, M. L. Wall, A. M. Rey, M. Foss-Feig, and J. J. Bollinger, *Quantum Spin Dynamics and Entanglement Generation with Hundreds of Trapped Ions*, Science **352**, 1297 (2016).
[10] A. Omran et al., *Generation and Manipulation of Schrödinger Cat States in Rydberg Atom Arrays*, Science **365**, 570 (2019).

Sources

GitHub repository: https://github.com/NGBigField/Superradiance